We are IntechOpen,
the world's leading publisher of
Open Access books
Built by scientists, for scientists

6,900
Open access books available

186,000
International authors and editors

200M
Downloads

Our authors are among the

154
Countries delivered to

TOP 1%
most cited scientists

12.2%
Contributors from top 500 universities

CLARIVATE ANALYTICS
BOOK CITATION INDEX
INDEXED

WEB OF SCIENCE™

Selection of our books indexed in the Book Citation Index
in Web of Science™ Core Collection (BKCI)

Interested in publishing with us?
Contact book.department@intechopen.com

Numbers displayed above are based on latest data collected.
For more information visit www.intechopen.com

Measurement Uncertainty of White-Light Interferometry on Optically Rough Surfaces

Pavel Pavlíček

Palacky University, Faculty of Science, Regional Centre of Advanced Technologies and Materials, Joint Laboratory of Optics of Palacky University and Institute of Physics of Academy of Science of the Czech Republic
Czech Republic

1. Introduction

White-light interferometry is an established method to measure the geometrical shape of objects. A typical setup for white-light interferometry is shown in Fig. 1.
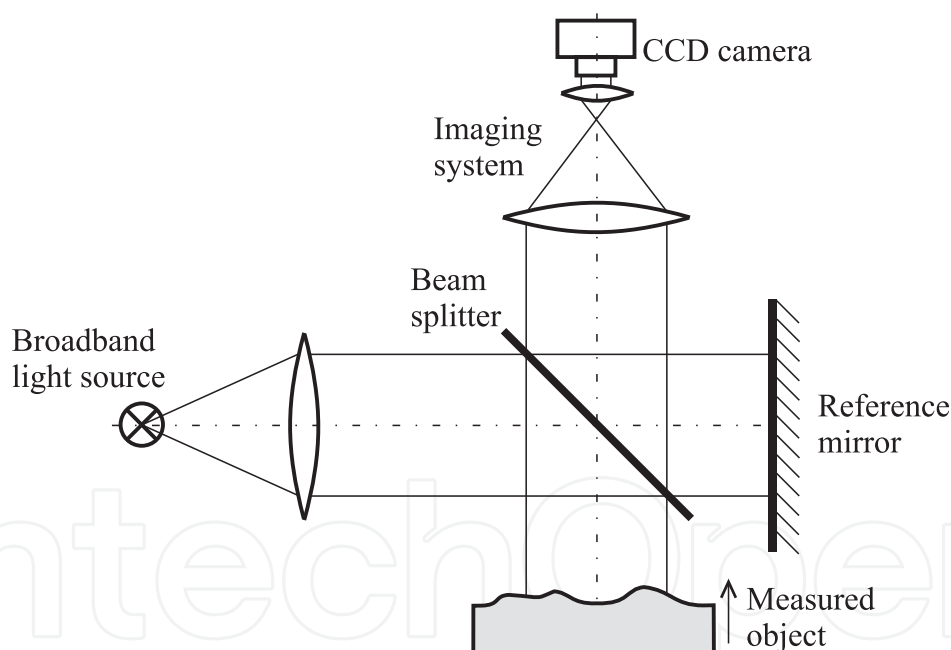

Fig. 1. Schematic of white-light interferometry.

A Michelson interferometer is illuminated by a broadband light source (e.g. light-emitting diode, superluminescent diode, arc or incandescent lamp). At the output of the interferometer, a CCD camera is used as a multiple detector. The measured object is placed in one arm of the interferometer and moved in the longitudinal direction as indicated by the arrow in Fig. 1. The surface of the object is imaged by a telecentric optical system onto the lightsensitive area of the CCD camera. During the moving of the object in the longitudinal direction, a series of images is acquired. From the acquired series, the coherence function (also referred to as correlogram or interferogram) can be extracted for each object point. The maximum of the

envelope of the correlogram is assigned to the longitudinal distance of the respective object point (Kino & Chim, 1990; Lee & Strand, 1990). A typical white-light correlogram is shown in Fig. 2.
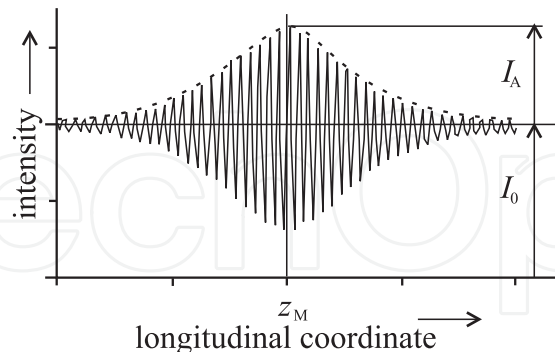

Fig. 2. Typical white-light correlogram.

Unlike to classical interferometry, white-light interferometry can be used for the measurement of the objects with an optically rough surface (Dresel et al., 1992). A surface is regarded as being optically rough when the standard deviation of the height variations within one resolution cell of the imaging system exceeds one-fourth of the wavelength of the used light. The property of the surface to be optically smooth or rough depends not only on the surface roughness but also on the wavelength of the used light and the size of the resolution cell of the imaging system (Häusler et al., 1999). In white-light interferometry on rough surface, the longitudinal distance of the object point is determined from the envelope of the correlogram only. The phase of the correlogram is not evaluated because it is a random quantity. The rough surface of the measured object implies the formation of speckle pattern in the image plane (on the lightsensitive area of the CCD camera).

In this work, we consider two influences that cause the measurement uncertainty: rough surface and the shot noise of the camera. The influence of rough surface on measurement uncertainty was described in our previous work (Pavlíček & Hýbl, 2008). It shows that the measurement uncertainty caused by surface roughness depends on the roughness and the intensity of individual speckle. The measurement uncertainty δz is given by the formula derived by T. Dresel (Dresel, 1991)

$$\delta z = \frac{1}{\sqrt{2}} \sqrt{\frac{\langle I_{\mathrm{obj}} \rangle}{I_{\mathrm{obj}}}} \, \sigma_h. \tag{1}$$

Here σ_h is the rms roughness of the surface, I_{obj} is the local intensity and $\langle I_{\mathrm{obj}} \rangle$ is the mean intensity of the speckle pattern. The subscript obj emphasizes that the intensities I_{obj}, $\langle I_{\mathrm{obj}} \rangle$ are meant with the shut reference arm (only the object arm is illuminated). Equation (1) indicates that the measurement of the longitudinal coordinate z is more precise for brighter speckles.

The intensity in the speckle pattern is distributed according to the gamma distribution (Parry, 1984)

$$p(I_{\mathrm{obj}}) = \frac{M^M I_{\mathrm{obj}}^{M-1}}{\langle I_{\mathrm{obj}} \rangle^M \Gamma(M)} \exp\left(-\frac{M I_{\mathrm{obj}}}{\langle I_{\mathrm{obj}} \rangle} \right), \tag{2}$$

where $\Gamma(\ )$ is the gamma function. The shape parameter M depends on the rms roughness σ_h and the coherence length l_c of the used light. For a light source with a Gaussian spectrum, the

shape parameter M is equal to

$$M = \sqrt{1 + 8\left(\frac{\sigma_h}{l_c}\right)^2}. \tag{3}$$

If the coherence length l_c is long and the rms roughness σ_h is small ($\sigma_h \lesssim \sqrt{8}l_c$), the gamma distribution differs only slightly from the negative exponential distribution (that corresponds to the monochromatic illumination)(Horváth et al., 2002). The coherence length l_c is related to the spectral width of the light source $\Delta\lambda$. For a spectral width $\Delta\lambda$ much lower than the central wavelength λ_0 of the light source, it holds (Pavlíček & Hýbl, 2008)

$$l_c \cong \frac{\sqrt{\ln 2}}{\pi}\frac{\lambda_0^2}{\Delta\lambda}. \tag{4}$$

The spectral width $\Delta\lambda$ in Eq. (4) is defined as full width at half maximum (FWHM).

George and Jain demonstrate that speckle patterns of two different wavelengths become decorrelated if the surface roughness exceeds a certain limit (George & Jain, 1973). A similar effect is observed with the speckle pattern produced by broadband light. If the rms roughness is high and the coherence length is short, the speckle becomes decorrelated. A decorrelated speckle implies a distorted correlogram. An example of a distorted correlogram is shown in Fig. 3.
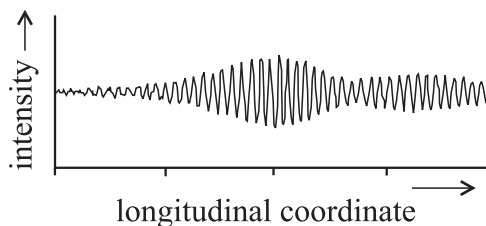

Fig. 3. Distorted white-light correlogram.

The limit beyond which the correlogram becomes distorted was found numerically (Pavlíček & Hýbl, 2008)

$$l_c < 4\sigma_h\sqrt{\frac{\langle I_{obj}\rangle}{I_{obj}}}. \tag{5}$$

The influence of the shot noise on the measurement uncertainty of white-light interferometry is described in (Pavlíček & Hýbl, 2011). The measurement uncertainty δz caused by shot noise is given by

$$\delta z = \sqrt{2}\sqrt[4]{\frac{2}{\pi}}\frac{N_{shot}}{I_A}\sqrt{\Delta z l_c}, \tag{6}$$

where N_{shot} is the intensity of the noise, I_A is the amplitude of the modulation of the correlogram, and Δz is the distance between two subsequent values of the coordinate z_O - the sampling step. The ratio N_{shot}/I_A is the noise-to-signal ratio and the meaning of I_A is shown in Fig. 2. The shot noise is caused by the uncertainty in counting the incoming photons. For a long integration time of the CCD camera (significantly longer than the coherence time of the used light), the photocount distribution can be assumed as Poissonian (Peřina, 1991). Then

$$N_{shot} = \sqrt{I}, \tag{7}$$

where I is the signal. Both N_{shot} and I are expressed in electrons. According to Eq. (7), the intensity N_{shot} of noise is different for each point of the correlogram. For a correlogram with the form as shown in Fig. 2, the intensity N_{shot} of noise in Eq. (7) can be replaced by the mean value $\overline{N_{shot}} = \sqrt{I_0}$. The meaning of the offset I_0 is shown in Fig. 2. The measurement uncertainty caused by the shot noise is then given by

$$\delta z = \sqrt{2} \sqrt[4]{\frac{2}{\pi}} \frac{\sqrt{I_0}}{I_A} \sqrt{\Delta z l_c}. \tag{8}$$

The intensities I_0 and I_A in Eq. (8) are again expressed in electrons.

Until now, the influence of both effects (rough surface and shot noise) have been studied separately. The goal of this work is to find the measurement uncertainty of white-light interferometry influenced by both effects. Similar to (Pavlíček & Hýbl, 2008), the calculations are performed numerically.

2. Assumptions

We understand the measurement uncertainty as the standard deviation of the distribution of the measurement error (the difference between the estimate and the true value). For the calculation of the error caused by surface roughness and shot noise, we take into consideration following assumptions:

1. The surface is macroscopically planar and microscopically rough. The height h_j of the j-th scattering center is a normally distributed random variable with zero mean. The standard deviation of the height distribution is equal to the rms roughness σ_h. The number of scattering centers inside of the resolution cell of the imaging system is n.

2. Because of the different reflectivity of the scattering centers, the amplitude a_j of the light reflected from j-th scattering center is a random variable obeying uniform distribution from 0 to A_M. The resultant amplitude of the light reflected from the measured surface is given by (Goodman, 1984)

$$\hat{A} = \sum_{j=1}^{n} \frac{a_j}{n^{1/2}} \exp(i2kh_j). \tag{9}$$

We assume that the amplitudes a_j and heights h_j are independent of each other and the amplitudes a_j do not depend on wave number k.

3. The spectral density of the broadband light has Gaussian form

$$S(k) = \frac{1}{2\sqrt{\pi}\Delta k} \exp\left[-\left(\frac{k - k_0}{2\Delta k}\right)^2\right], \tag{10}$$

where $k_0 = 2\pi/\lambda_0$ is the central wave number and $\Delta k = 1/(2l_c)$ is the effective band width in wave number units (Born & Wolf, 2003). The effective bandwidth Δk can be calculated from the spectral width $\Delta\lambda$ by means of Eq. (4).

4. The noise is a signal-independent normally distributed random variable with zero mean and standard deviation $\overline{N_{shot}}$.

3. Simulation

3.1 Generation of the correlogram

The phasor amplitude of light having passed through the object arm with the rough surface is, according to Eq. (9), given by

$$\hat{A}(k, z_O) = \sum_{j=1}^{n} \frac{a_j}{n^{1/2}} \exp[i2k(z_O + h_j)]. \tag{11}$$

The position z_O of the rough surface is given by the position of the mean value of height distribution as shown in Fig. 4.
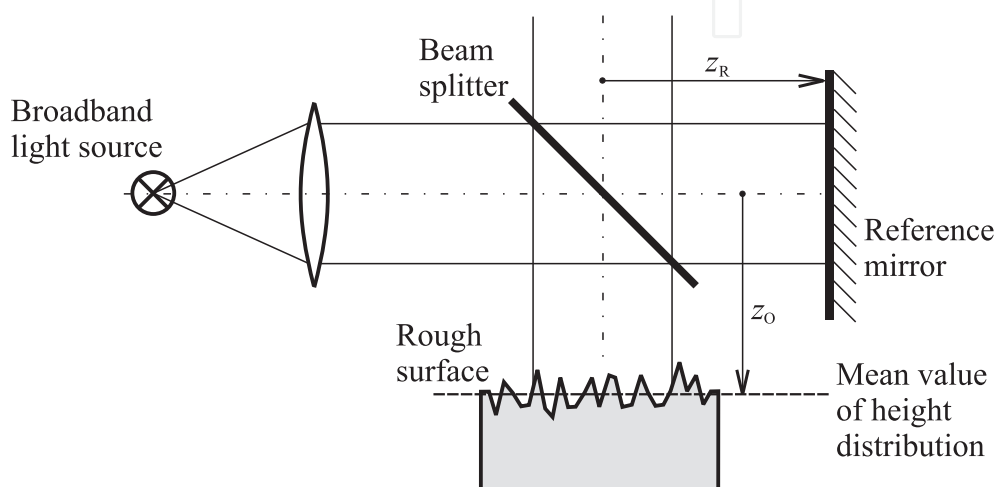

Fig. 4. Object and reference arm of the setup for white-light interferometry.

The phasor amplitude of light having passed the reference arm with the reference mirror is given by

$$\hat{B}(k, z_R) = B \exp(i2kz_R), \tag{12}$$

where B is the amplitude of light in the reference arm and z_R is the position of the reference mirror. The meaning of both the positions z_O and z_R follows from Fig. 4.

The light intensity at the interferometer output is given by

$$I_k(k, z_O - z_R) = |\hat{A}(k, z_O) + \hat{B}(k, z_R)|^2. \tag{13}$$

The subscript k means that I_k is the intensity calculated for the wave number k. To obtain the total intensity at the output of the interferometer, I_k must be integrated over all wave numbers. Because the light components with various wave numbers are not uniformly distributed in the spectrum, I_k must be multiplied by spectral density $S(k)$. Theoretically, the integration should be performed over the whole interval $(-\infty, \infty)$. However, the integration is calculated numerically and therefore we restrict the calculation on a finite interval which corresponds to three standard deviations on each side from the central wave number: $k_{min} = k_0 - 3\sqrt{2}\Delta k, k_{max} = k_0 + 3\sqrt{2}\Delta k$

$$I(z_O - z_R) = \int_{k_{min}}^{k_{max}} S(k) I_k(k, z_O - z_R) dk. \tag{14}$$

The integration in Eq. (14) is transformed to a sum

$$I(z_O - z_R) = \sqrt{\frac{2}{\pi}} \frac{3}{n_k} \sum_{l=1}^{n_k} \exp\left[-\left(\frac{k_l - k_0}{2\Delta k}\right)^2\right] I_k(k_l, z_O - z_R) \tag{15}$$

with

$$k_l = \frac{l - 1/2}{n_k}(k_{max} - k_{min}) + k_{min}. \tag{16}$$

In Eqs. (15) and (16), n_k is the number of used wave numbers.

Equation (15) for the intensity I expressed as a function of the coordinate z_O, while the coordinate z_R is constant, describes the correlogram. The correlogram is calculated for n_c points (values of the coordinate z_O). The calculated correlogram is superposed by the noise with normal distribution and a constant (signal independent) standard deviation $\overline{N_{shot}}$.

$$I_n(z_m) = I(z_m) + N_m \tag{17}$$

with $z_m = m\Delta z$ for $m = 1, ..., n_c$.

The local intensity I_{obj} of the speckle pattern that appears in Eqs. (1), (2), and (5) can be calculated from Eq. (15) for $B = 0$ (the reference arm is shut) and an arbitrary value of z_O. Because the expression for I_{obj} contains no interference term, it does not depend on the coordinate z_O. For simplicity we choose $z_O = z_R$

$$I_{obj} = \sqrt{\frac{2}{\pi}} \frac{3}{n_k} \sum_{l=1}^{n_k} \exp\left[-\left(\frac{k_l - k_0}{2\Delta k}\right)^2\right] \left[\left(\sum_{j=1}^{n} \frac{a_j}{\sqrt{n}} \cos(2k_l h_j)\right)^2 + \left(\sum_{j=1}^{n} \frac{a_j}{\sqrt{n}} \sin(2k_l h_j)\right)^2\right]. \tag{18}$$

The mean intensity of the speckle pattern is given by

$$\langle I_{obj}\rangle = \langle a_j^2\rangle. \tag{19}$$

According to Eq. (12), the intensity of the reference beam is

$$I_{ref} = B^2. \tag{20}$$

Thus the amplitude of the modulation is given by

$$I_A = 2B\sqrt{I_{obj}} \tag{21}$$

and the noise-to-signal ratio is equal to

$$NSR = \frac{N_{shot}}{2B\sqrt{I_{obj}}}. \tag{22}$$

If the amplitudes $\{a_j\}$ obey uniform distribution from 0 to A_M as postulated in assumption 2 in Sec. 2

$$\langle I_{obj}\rangle = \frac{1}{3}A_M^2 \tag{23}$$

and

$$NSR = \frac{\sqrt{3}}{2}\sqrt{\frac{\langle I_{obj}\rangle}{I_{obj}}}\frac{N_{shot}}{A_M B}. \tag{24}$$

The heights $\{h_j\}$, amplitudes $\{a_j\}$ and noise values $\{N_m\}$ used for the simulation are random numbers. The random numbers have been generated by quantum random number generator developed in the Joint Laboratory of Optics (Soubusta et al., 2003).

3.2 Evaluation of the correlogram

The obtained noised correlogram is evaluated to find the "measured" value z_M of the surface. The value z_M is determined from the maximum of the envelope of the correlogram. The meaning of z_M is shown in Fig. 2.

The envelope of the correlogram is calculated using a discrete Hilbert transform. The calculation of the envelope can be described in five steps (Onodera et al., 2005). In the first step, the mean intensity I_0 is subtracted from the correlogram. In this way, the zero mean correlogram is obtained. In the second step, the zero mean correlogram is Fourier transformed. In the third step, the Fourier transform is multiplied by the imaginary unit (i) for positive frequencies and by the negative of the imaginary unit (-i) for negative frequencies. In the fourth step, the result is inversely Fourier transformed. Thus the Hilbert transform of the zero mean correlogram is obtained. The Hilbert transform of the correlogram alters its phase by $\pi/2$. Finally, in the fifth step, the Hilbert transform of the zero mean correlogram is squared and added to the square of the zero mean correlogram itself for each value of z_O. The square root of this sum is the value of the envelope of the correlogram for the given value of z_O.

The position z_M of the maximum of the envelope is estimated by use of the least-squares method (Press et al., 1992). The sought measurement error is the difference between the estimate and the true value. Without the influence of surface roughness and shot noise, the maximum of the envelope would be located at $z_M = z_R$. Therefore, the measurement error is mathematically expressed by

$$\Delta = z_M - z_R. \tag{25}$$

4. Results of the simulation

Here the results of the simulation are presented. The quantities are calculated numerically for n_s speckles, each of them calculated using a set of values $\{h_j\}$, $\{a_j\}$, and $\{N_m\}$; $j = 1, 2, ..., n$, $m = 1, 2, ..., n_c$. The sets $\{h_j\}$ have a normal distribution with the standard deviation σ_h. The sets $\{a_j\}$ have a uniform distribution from 0 to A_M and the sets $\{N_m\}$ have a normal distribution with the standard deviation $\overline{N_{shot}}$.

4.1 Distribution of the intensity

First, the attention is given to the intensity distribution in the object arm. Intensity I_{obj} is calculated from Eqs. (15), (13), and (11) with $B = 0$ and $z_O = z_R$. The parameters of the simulation are $n_s = 20\,000$, $n = 200$, $n_k = 200$, $A_M = 1$.

Figure 5 displays the results of the calculated intensity distribution for $\lambda_0 = 820nm$, $\sigma_h = 1.2\mu m$, and three values of spectral width $\Delta\lambda = 10, 38$, and $80nm$.

The numerically calculated results are compared with the solutions obtained from Eq. (2). The gamma distribution described by Eq. (2) is plotted in Fig. 5 with a dashed curve. The numerically obtained results are in good agreement with the analytical solutions as follows from Fig. 5. The variance of the intensity distribution described by Eq. (2) is equal to

$$\text{var}\{I_{obj}\} = \frac{\langle I_{obj}\rangle^2}{M}. \tag{26}$$

The contrast of the speckle pattern is given by (Parry, 1984)

$$C = \frac{\sqrt{\text{var}\{I_{obj}\}}}{\langle I_{obj}\rangle} \tag{27}$$
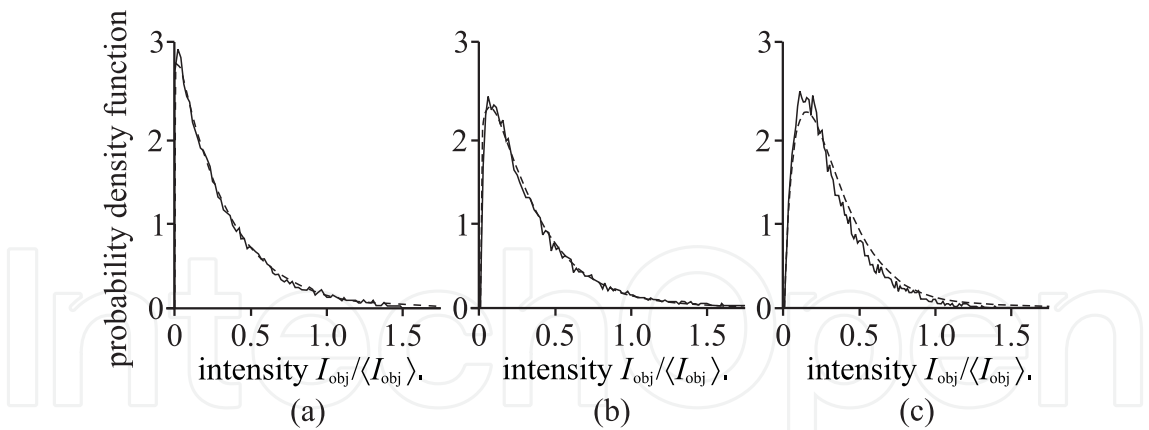
Fig. 5. Intensity distribution for $\lambda_0 = 820nm$, $\sigma_h = 1.2\mu m$. (a) $\Delta\lambda = 10nm$. (b) $\Delta\lambda = 38nm$. (c) $\Delta\lambda = 80nm$.

and from Eq. (26), it follows

$$C = \frac{1}{\sqrt{M}}. \tag{28}$$

In Table 1, the values of contrast C_{num} calculated numerically from Eq. (27) are compared with the values of contrast C obtained by means of Eqs. (3) and (28). Because $A_M = 1$, the mean

$\Delta\lambda(nm)$	$l_c(\mu m)$	$\langle I_{\text{obj}}\rangle$	$\text{var}\{I_{\text{obj}}\}$	C_{num}	C
10	17.8	0.335	0.110	0.99	0.99
20	8.9	0.333	0.106	0.98	0.97
30	5.9	0.333	0.097	0.94	0.93
40	4.5	0.333	0.089	0.90	0.89
50	3.6	0.335	0.081	0.85	0.85
60	3.0	0.334	0.074	0.81	0.81
70	2.5	0.335	0.066	0.77	0.77
80	2.2	0.336	0.062	0.74	0.74

Table 1. Numerically calculated speckle contrast for various spectral widths of the light source ($\lambda_0 = 820nm$, $\sigma_h = 1.2\mu m$)

intensity $\langle I_{\text{obj}}\rangle$ of the speckle pattern is equal approximately to $1/3$ according to Eq. (23). The dependence of the contrast C_{num} on the spectral width $\Delta\lambda$ is plotted in Fig. 6(a). This dependence is an analogy to the dependence of the contrast on the illumination aperture as described in (Häusler, 2005). For comparison, the dependence of the contrast on the illumination aperture is illustrated in Fig. 6(b).

4.2 Distribution of the measurement error
The distribution of the measurement error caused by surface roughness and shot noise is calculated numerically using Eq. (25). The parameters of the simulation are $n_s = 20\,000$, $n_c = 1024$, $n = 200$, $n_k = 200$, $A_M = 1$, $B = 1$. As an example, the distribution of the measurement error is calculated for $\lambda_0 = 820nm$, $\Delta\lambda = 35nm$, $\sigma_h = 0.4\mu m$, $I_{\text{obj}} = \langle I_{\text{obj}}\rangle$, $\Delta z = \lambda_0/10$, and $N_{\text{shot}} = 0.0577$. The relation $I_{\text{obj}} = \langle I_{\text{obj}}\rangle$ means that only those cases are entered into the statistics when the intensity I_{obj} falls into a certain neighborhood of the mean intensity $\langle I_{\text{obj}}\rangle$. The noise-to-signal ratio is equal to NSR = 0.05 according to Eq. (24). The results of the calculation are presented in Fig. 7.
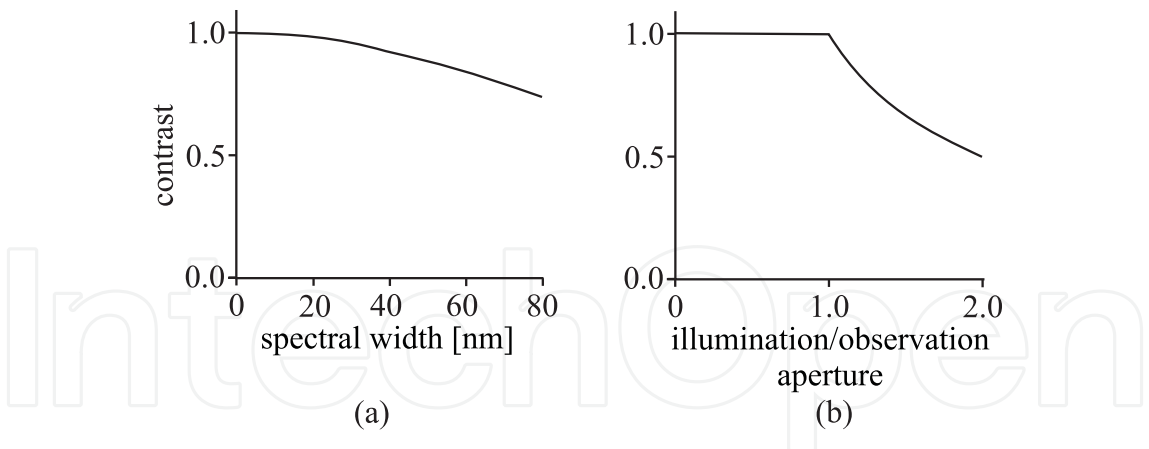
Fig. 6. (a) Speckle contrast as a function of spectral width (numerically calculated data) for $\lambda_0 = 820nm$, $\sigma_h = 1.2\mu m$. (b) Speckle contrast as a function of illumination aperture according to Häusler.
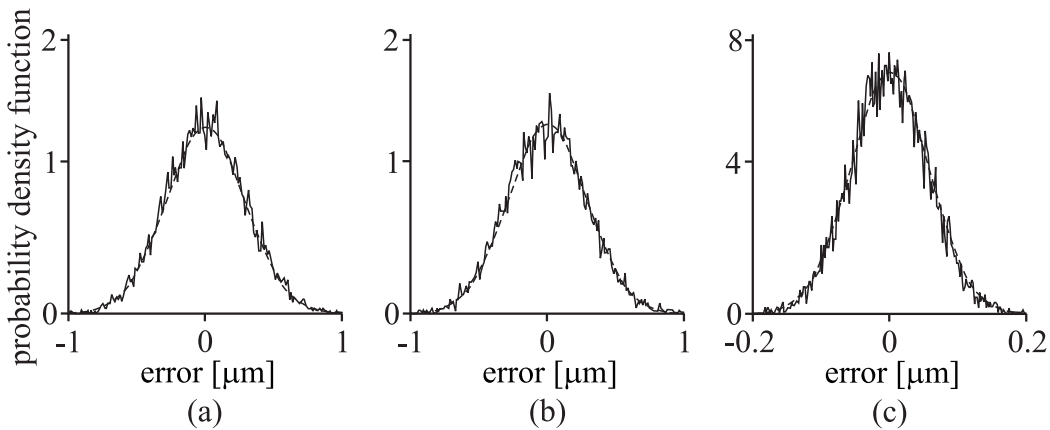

Fig. 7. Distribution of the measurement error for $\lambda_0 = 820nm$, $\Delta\lambda = 35nm$, $\sigma_h = 0.4\mu m$, $I_{obj} = \langle I_{obj} \rangle$, and NSR $= 0.05$. (a) Error caused by surface roughness and shot noise. (b) Error caused by surface roughness only. (c) Error caused by shot noise only.

The distribution of the measurement error for the noised correlogram on rough surface is shown in Fig. 7(a). Figure 7(b) shows the distribution of the measurement error for the correlogram without noise. Finally, the distribution of the measurement error for the noised correlogram on smooth surface is illustrated in Fig. 7(c). It shows up that the distribution of the measurement error tends in all three cases to a normal distribution centered at zero. For comparing, the shape of the normal distribution is plotted by dashed line in Fig. 7. The zero mean of the calculated distribution means that the expected value of the measured coordinate is the mean value of height distribution within the resolution cell. The standard deviation of the calculated distribution is the sought measurement uncertainty. In the given example, the numerically calculated measurement uncertainties are $\delta z = 0.293\mu m$, $\delta z_{rough} = 0.288\mu m$, and $\delta z_{noise} = 0.055\mu m$ for the cases shown in Figs. 7(a), 7(b), and 7(c), respectively. It is apparent that it holds

$$(\delta z)^2 = (\delta z_{rough})^2 + (\delta z_{noise})^2. \tag{29}$$

This result is to be expected, because the influences of the noise and of the rough surface are independent. A sum of two independent random variables with normal distribution and

the standard deviations equal to σ_A and σ_B, respectively, is a random variable with normal distribution and standard deviation equal to $\sigma = \sqrt{\sigma_A^2 + \sigma_B^2}$.

The numerically calculated measurement uncertainties are compared with the theoretical values calculated from Eqs. (1) and (6). For the abovementioned example, the theoretical results are $\delta z = 0.286\mu m$, $\delta z_{\text{rough}} = 0.283\mu m$, and $\delta z_{\text{noise}} = 0.041\mu m$ which is in a good agreement with the numerical calculations. The numerically calculated value of δz_{noise} is higher than the theoretical prediction. The reason is that the fit is performed on a limited interval of the longitudinal coordinate ($-\sqrt{3/2}l_c < z_O - z_M < \sqrt{3/2}l_c$). The numerical calculations for other values of λ_0, $\Delta\lambda$, σ_h, I_{obj}, Δz, and N_{shot} confirm the validity of Eq. (29). By comparing the values δz_{rough} and δz_{noise}, it is apparent that the influence of rough surface is significantly higher for "usual" values of spectral width, sampling step and noise-to-signal ratio. However, when white-light interferometry is operated with a narrow-band light source or with an extremely long sampling step, the influence of noise will increase. Equations (1) and (6) enable to compare the influences of both effects.

4.3 Measurement uncertainty

The measurement uncertainty caused by surface roughness and shot noise is calculated as function of the spectral widht $\Delta\lambda$. The parameters of the simulation are $n_s = 10\,000$, $n_c = 1024$, $n = 200$, $n_k = 200$, $A_M = 1$, $B = 1$. Figure 8 shows the result for $\lambda_0 = 820nm$, $\sigma_h = 1.2\mu m$, $I_{\text{obj}} = \langle I_{\text{obj}} \rangle$, and NSR = 0.05 as an example.
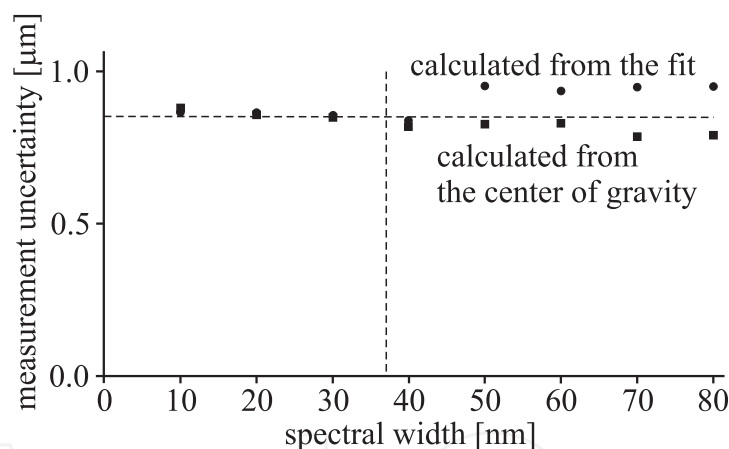

Fig. 8. Numerically calculated measurement uncertainty δz as a function of spectral width $\Delta\lambda$ for $\lambda_0 = 820nm$, $\sigma_h = 1.2\mu m$, $I_{\text{obj}} = \langle I_{\text{obj}} \rangle$, and NSR = 0.05.

The circles indicate the values calculated from the fit using the least-squares method. The squares correspond to the values calculated from the center of gravity of the correlogram envelope (Pavlíček & Hýbl, 2008). For small values of the spectral width, both methods yield approximately same results. The numerically calculated measurement uncertainty corresponds to the value calculated using Eqs. (29), (1), and (6). This value is indicated by the horizontal dashed line for the respective values of σ_h, I_{obj}, and NSR. In fact, the line is slightly inclined because the measurement uncertainty caused by shot noise depends on spectral width of the used light according to Eq. (6).

After the spectral width exceeds the spectral width corresponding to the limit coherence length given by Eq. (5), the values calculated from the fit begin to differ from those calculated from the center of gravity. The limit spectral width for the respective values of σ_h and I_{obj} is indicated by the vertical dashed line in Fig. 8. The measurement uncertainty calculated

from the fit begins to increase. The reason is the distortion of the correlogram as shown in Fig. 3. The fitting of the envelope and its evaluation by means of least-squares method is no more as accurate as for an undistorted correlogram. On the other hand, the evaluation of a distorted correlogram by means of the center of gravity is more accurate than that of an undistorted correlogram (Pavlíček & Hýbl, 2008). For a light source with an extremely large spectral width $\Delta\lambda = 120nm$ (other conditions are the same as above), the measurement uncertainty calculated from the center of gravity sinks to $0.770\mu m$.

5. Conclusion

The influence of rough surface and shot noise on measurement uncertainty of white-light interferometry on rough surface has been investigated. It has shown that both components of measurement uncertainty add geometrically. The numerical simulations have shown that the influence of the rough surface on the measurement uncertainty is for usual values of spectral width, sampling step and noise-to-signal ratio significantly higher than that of shot noise. The influence of rough surface prevails over the influence of shot noise. The obtained results determine limits under which the conditions for white-light interferometry can be regarded as usual. For low values of spectral width and high values of sampling step and noise-to-signal ratio, the influence of the noise must be taken into account.

6. Acknowledgement

7. References

Born, M. & Wolf, E. (2003). *Principles of Optics*, Cambridge University Press, Cambridge.

Dresel, T. (1991). *Grundlagen und Grenzen der 3D-Datengewinnung*, Master's thesis, University Erlangen-Nuremberg, Erlangen.

Dresel, T., Häusler, G. & Venzke, H. (1992). Three-dimensional sensing of rough surfaces by coherence radar, *Applied Optics* Vol. 31 (No. 7): 919–925.

George, N. & Jain, A. (1973). Speckle reduction using multiple tones of illumination, *Applied Optics* Vol. 12 (No. 6): 1202–1212.

Goodman, J. W. (1984). Statistical properties of laser speckle patterns, *in* Dainty, J. C. (ed.), *Speckle and Related Phenomena*, Springer-Verlag, pp. 9–75.

Häusler, G., Ettl, P., Schenk, M., Bohn, G. & László, I. (1999). Limits of optical range sensors and how to exploit them, *in International Trends in Optics and Photonics ICO IV*, Vol. 74 Springer Series in Optical Sciences, Springer-Verlag, Berlin, pp. 328–342.

Häusler, G. (2005). Speckle and coherence, *in* Guenther, B. D. (ed.), *Encyclopedia of Modern Optics*, Elsevier, Academic Press, Amsterdam, pp. 114–123.

Horváth, P., Hrabovský, M. & Bača, Z. (2002). Statistical properties of a speckle pattern, *in Proc. SPIE*, Vol. 4888, pp. 99–108.

Kino, G. S. & Chim, S. S. C. (1990). Mirau correlation microscope, *Applied Optics* Vol. 29 (No. 26): 3775–3783.

Lee, B. S. & Strand, T. C. (1990). Profilometry with a coherence scanning microscope, *Applied Optics* Vol. 29 (No. 26): 3784–3788.

Onodera, R., Watanebe, H. & Ishii, Y. (2005). Interferometric phase-measurement using a one-dimensional discrete Hilbert transform, *Optical Rewiev* Vol. 12 (No. 1): 29–36.

Parry, G. (1984). Speckle patterns in partially coherent light, *in* Dainty, J. C. (ed.), *Speckle and Related Phenomena*, Springer-Verlag, pp. 77–121.

Pavlíček, P. & Hýbl, O. (2008). White-light interferometry on rough surfaces – measurement uncertainty caused by surface roughness, *Applied Optics* Vol. 47 (No. 16): 2941–2949.

Pavlíček, P. & Hýbl, O. (2011). Pavlíček, P. Palacky University, Faculty of Science, Regional Centre of Advanced Technologies and Materials, Joint Laboratory of Optics of Palacky University and Institute of Physics of Academy of Science of the Czech Republic, & Hýbl, O. are preparing a manuscript to be called: Theoretical limits of the measurement uncertainty of white-light interferometry.

Peřina, J. (1991). *Quantum statistics of linear and nonlinear optical phenomena*, Kluwer Academic Publishers, Dordrecht.

Press, W. H., Teukolsky, S. A., Vettering W. T. & Flannery B. P. (1992). *Numerical Recipes in C: The Art of Scientific Computing*, Cambridge University Press, Cambridge.

Soubusta, J., Haderka, O., Hendrych, M. & Pavlíček, P. (2003). Experimental realization of quantum random generator, *in Proc. SPIE*, Vol. 5259, pp. 7–13.
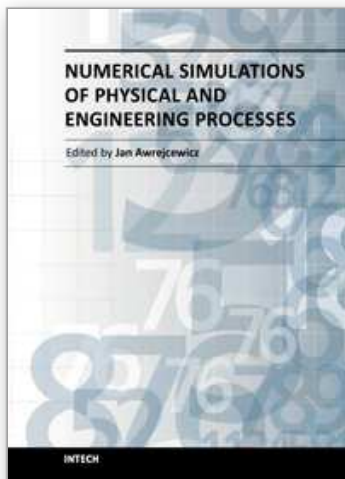
Numerical Simulations of Physical and Engineering Processes

Edited by Prof. Jan Awrejcewicz

Numerical Simulations of Physical and Engineering Process is an edited book divided into two parts. Part I devoted to Physical Processes contains 14 chapters, whereas Part II titled Engineering Processes has 13 contributions. The book handles the recent research devoted to numerical simulations of physical and engineering systems. It can be treated as a bridge linking various numerical approaches of two closely inter-related branches of science, i.e. physics and engineering. Since the numerical simulations play a key role in both theoretical and application oriented research, professional reference books are highly needed by pure research scientists, applied mathematicians, engineers as well post-graduate students. In other words, it is expected that the book will serve as an effective tool in training the mentioned groups of researchers and beyond.

INTECH
open science | open minds